ARTICLE

Hydrothermal Synthesis and Efficient Visible Light Photocatalytic Properties of $InVO_4$ Hierarchical Microspheres and $InVO_4$ Nanowires

Xue Lin[a*], Shi-duo Zhao[b], Xiao-yu Guo[b], Xin Gao[b], Jiu-jing Shi[b], Yi-li Liu[b], Hong-ju Zhai[a], Qing-wei Wang[b]

a. Key Laboratory of Preparation and Application of Environmentally Friendly Materials, Ministry of Education, Jilin Normal University, Siping 136000, China
b. College of Chemistry, Jilin Normal University, Siping 136000, China

(Dated: Received on March 13, 2014; Accepted on May 14, 2014)

In this work, $InVO_4$ hierarchical microspheres and $InVO_4$ nanowires were successfully synthesized by a facile hydrothermal method. Field emission scanning electron microscopy showed that $InVO_4$ crystals can be fabricated in different morphologies by simply manipulating the reaction parameters of hydrothermal process. The as-prepared $InVO_4$ photocatalysts exhibited higher photocatalytic activities in the degradation of rhodamine B under visible-light irradiation (λ>420 nm) compared with commercial P25 TiO_2. Furthermore, the as-synthesized $InVO_4$ hierarchical microspheres showed higher photocatalytic activity than that of $InVO_4$ nanowires. Up to 100% Rh B (3 μmol/L) was decolorized after visible-light irradiation for 40 min. In addition, the reason for the difference in the photocatalytic activities for $InVO_4$ hierarchical microspheres and $InVO_4$ nanowires was studied based on their structures and morphologies.

Key words: Photocatalysis, $InVO_4$, Nanowires, Microspheres, Visible-light irradiation

I. INTRODUCTION

Semiconductor photocatalysis has been broadly studied as a promising method for environmental remediation. TiO_2 as the most widely used material in the pollution control has attracted much attention due to its high photocatalytic acitivity, excellent stability for chemical and photocorrosions, commercial availability, and low price [1−4]. However, anatase TiO_2 is responsive only towards UV light, which represents a small fraction (ca. 4%) of the sunlight. Therefore, it is of significance to develop visible-light driven photocatalytic materials [5−11].

$InVO_4$ is a novel photocatalyst for water splitting and organic pollutant photodegradation under visible-light irradiation [12−16]. Recently, a great number of investigations have been focused on the preparation of $InVO_4$. Several methods, such as solid-state reaction[17, 18], coprecipitation[19, 20], hydrothermal treatment[21], solgel reaction[22], and template-directing selfassembling methods [23], have been developed to synthesize monoclinic or orthor-hombic $InVO_4$ with different morphologies. Among the various pathways, hydrothermal synthesis as a soft-chemical process has been widely used in the preparation of many kinds of functional materials [24]. The experimental paramters in hydrothermal synthesis, such as the concentrations of reactants, the pH values, the temperature, and the reaction medium, can be easily tuned to control the microstructures, and thus the properties and property dependent applications of the target materials.

Herein, we reported a low-temperature solution-phase route to synthesize $InVO_4$ photocatalysts. The photodegradation of rhodamine B (Rh B) was employed to evaluate the photocatalytic activities of the as-prepared $InVO_4$ samples under visible-light irradiation (λ>420 nm). It was demonstrated that the $InVO_4$ hierarchical microspheres showed excellent photocatalytic performance. For the degradation of Rh B (3 μmol/L) under visible-light irradiation, almost 100% of the Rh B was degraded within 40 min.

II. EXPERIMENTS

A. Preparation of $InVO_4$ photocatalysts

All reagents were of analytical purity and used without further purification. In a typical synthesis of $InVO_4$, 2 mmol of $In(NO_3)_3{\cdot}4.5H_2O$ was dispersed into 10 mL of distilled water and 1 mL HNO_3 (65wt%). Then an emulsion of $NaVO_3{\cdot}H_2O$ (1 mmol of $NaVO_3$, 10 mL of distilled water) was added to the above mixture under magnetic stirring. The amorphous yellow slurry formed immediately. The yellow slurry was separated into two parts (denoted as S1). Then, 0.03 g of sodium dodecyl benzene sulfonate (SDBS) was added

*Author to whom correspondence should be addressed. E-mail: jlsdlinxue@126.com, FAX: +86-434-3291890

into one of the two parts. The pH value of the two parts was adjusted with NaOH solution to 4. Then the two parts were transferred into two 20 mL Teflon-lined autoclaves, re-spectively. Subsequently, the autoclaves were heated to 150 °C in an oven. After crystallizing for 24 h, the resulting yellow products were filtered, washed with et-hanol, distilled water several times, and dried at 100 °C for 2 h (denoted as S2).

B. Characterization of $InVO_4$ photocatalysts

The crystal structures of the samples were characterized by X-ray diffraction (XRD) on a Rigaku D/max 2500 X-ray diffractometer (Cu Kα radiation, λ=0.15418 nm). A field emission scanning electron microscopy Field emission scanning electron microscopy (FESEM, Japan Electron Optics Laboratory Co. Ltd. JSM-6700F) was employed to observe the surface morphologies of the resulting samples. The specific surface areas of $InVO_4$ samples were measured through N_2 adsorption Brunauer-Emmett-Teller (BET) method (BET/Barrett-Joyner-Halenda (BJH) Surface Area, 3H-2000PS1). The diffuse reflectance spectra (DRS) were measured by a UV-Vis spectrometer (UV-2550, Shimadzu). $BaSO_4$ was used as the reflectance standard material.

C. Photocatalytic activities

The photocatalytic activities of $InVO_4$ samples were evaluated using Rh B dye as a model compound. In experiments, the Rh B dye solution (3 μmol/L, 100 mL) containing 0.02 g of $InVO_4$ photocatalyst were mixed in a pyrex reaction glass. A 500 W Xe lamp (λ>420 nm) was used to provide visible-light irradiation. A glass sheet was inserted between the lamp and the sample to filter out UV light (λ<420 nm). Prior to illumination, the suspension was strongly magnetically stirred for 30 min in the dark for adsorption/desorption equilibrium. Then the solution was exposed to visible-light irradiation under magnetic stirring. At given time intervals, about 4 mL of the suspension was periodically withdrawn and analyzed after centrifugation. The Rh B concentration was analyzed by a UV-2550 spectrometer to record intensity of the maximum band at 552 nm in the UV-Vis absorption spectra.

III. RESULTS AND DISCUSSION

Figure 1 shows the XRD patterns of the as-prepared $InVO_4$ samples prepared by hydrothermal procedure at different reaction parameters. All diffraction peaks can be assigned to the orthorhombic $InVO_4$ (JCPDS No.48-0898). No peaks of impurities were detected from these patterns. The strong and sharp peaks indicate high crystallinity of the samples. Furthermore, S2 has stronger peak intensity which means the crystallinity of S2 was higher compared to S1.

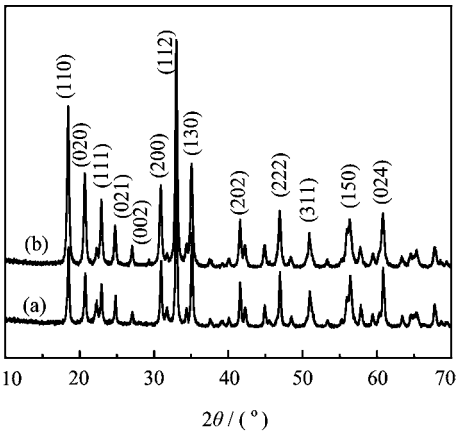

FIG. 1 XRD patterns of the as-prepared $InVO_4$ samples (a) S1 and (b) S2.

FESEM was used to observe the morphologies of the as-fabricated $InVO_4$ products. Figure 2(a) is a typical low-magnification SEM image of $InVO_4$ sample S1, from which a number of uniform microspheres with average diameter of aroud 3 μm can be clearly observed. No other morphologies are detected, indicating a high yield of these microspheres. High-magnification SEM image in Fig.2(b) clearly shows the rough surface of the microspheres and some detailed structural information of the S1 sample. The microspheres were constructed of numerous spherical naoparticles. These nanoparticles were densely selfassembled and formed 3D hierarchical structures. Figure 2(c) reveals that the morphology of $InVO_4$ sample obtained without any SDBS assisted (S2) is nanowires with average width of about 100 nm and lengths up to several micrometres. It shows that different shape of $InVO_4$ nanostructures with or without the SDBS assisted can be obtained in Fig.3. In the case of SDBS-mediated synthesis, part of the surfactant molecules were adsorbed on the surface of the $InVO_4$ nuclei to decrease the surface energy of the nanocrystals. The adsorbed SDBS might work as a capping agent to decrease the growth rate of the adsorbed crystal faces, thus forming 3D hierarchical $InVO_4$ nanostructures. In the case of surfactant-free synthesis, after 24 h reaction, the particles self-assembled according to the preferential orientation at pH value of 4, and finally crystallized into 1D thread-like nanostructures. Thus, $InVO_4$ crystals can be fabricated in different morphologies by simply manipulating the reaction parameters of hydrothermal process.

The UV-Vis DRS of the as-obtained $InVO_4$ samples are shown in Fig.4. The as-prepared $InVO_4$ samples show absorption bands in the visible-light region of the electromagnetic spectra, which is the characteristic absorption of orthorhombic $InVO_4$ [13]. The steep absorp-

DOI:10.1063/1674-0068/27/04/428-432

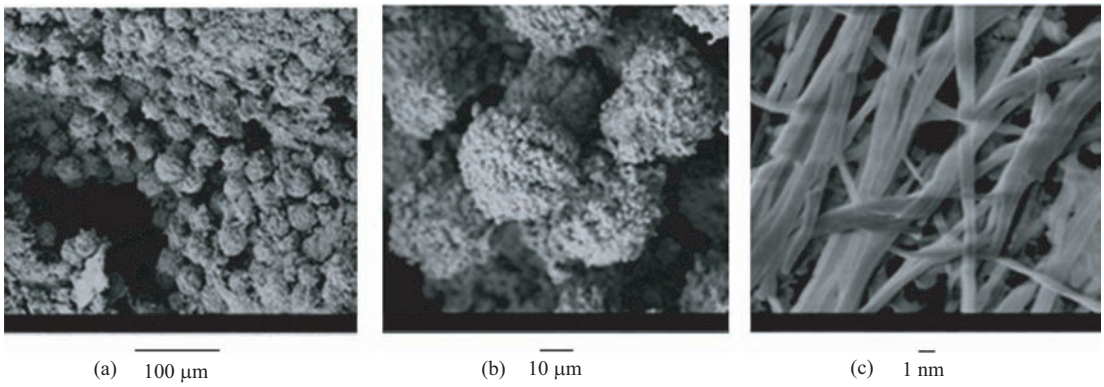

FIG. 2 SEM images of the as-prepared $InVO_4$ samples. (a, b) S1, and (c) S2.

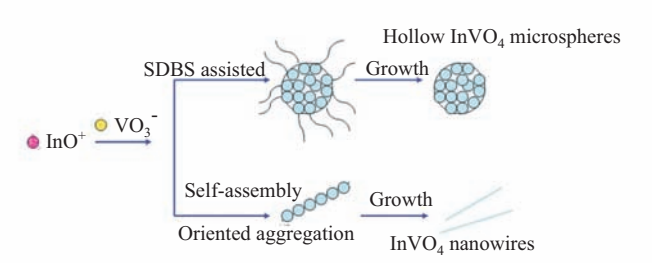

FIG. 3 Schematic illustration of the syntheses of different morphologies of $InVO_4$ crystals.

tion edge in the visible range indicates that the absorption of visible light is due to not the transition from impurity levels but the band gap transition [25]. However, shifts in the absorption edges between the two samples were observed. The absorption edge of S2 shifted to shorter wavelengths (*i.e.* blue-shifted). The band gap energy (E_g) played an important role in photocatalysis. It was convenient to use E_g to evaluate the optical absorption performance of photo-responsive materials. For a crystal semiconductor, the optical absorption near the band edge obeyed the following equation:

$$\alpha h\nu = A(h\nu - E_g)^{n/2} \quad (1)$$

in which A, α, and $h\nu$ represent constant, absorption coefficient, and incident photon energy [23], respectively. The n value depends upon the characteristics of the transition in a semiconductor: n=1 for direct transition and n=4 for indirect transition. According to the intercepts of the $(\alpha h\nu)^2$ versus $h\nu$ curves (as shown in Fig.4(b)) of the $InVO_4$ samples, one can obtain E_g values, which were ca. 1.91 and 2.63 eV for S1 and S2 respectively. These data clearly demonstrate that the electronic structures of $InVO_4$ were changed under different conditions. The variations in the electronic structures led to different degrees of delocalization of photogenerated electrons and holes pairs, which therefore resulted in different mobilities of photogenerated holes [23]. The lower band gap energy of the S1 sample would render its higher photocatalytic activity in the

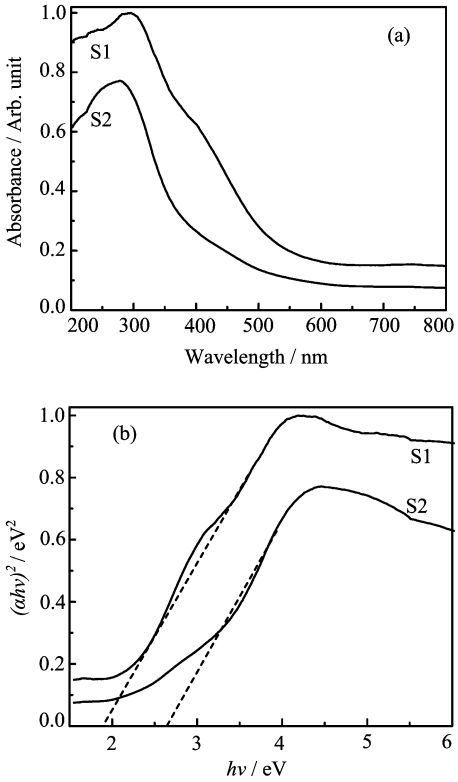

FIG. 4 (a) UV-Vis DRS and (b) the plot of $(\alpha h\nu)^2$ versus photon energy ($h\nu$) for the band-gap energies of the as-prepared $InVO_4$ samples.

degradation of Rh B under visible-light illumination.

Photodegradation experiments of Rh B were carried out under visible-light irradiation in order to test the photocatalytic properties of $InVO_4$ photocatalysts. The temporal evolutions of the spectral changes during the photodegradation of Rh B over $InVO_4$ samples under visible light illumination are displayed in Fig.5. It can be concluded that the degradation rate of Rh B mediated by S1 is much faster than that mediated by S2. The photodegradation for the two kinds of $InVO_4$ sam-

DOI:10.1063/1674-0068/27/04/428-432

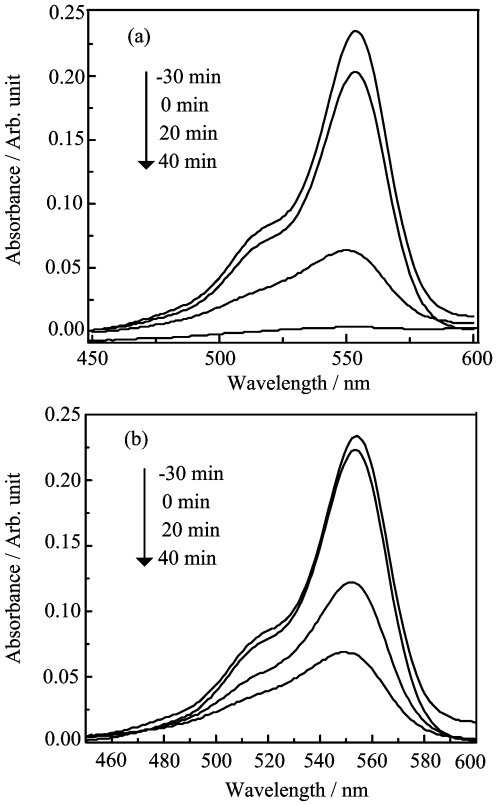

FIG. 5 UV-Vis absorption spectra of RhB in the presence of $InVO_4$ samples before irradiation of 30 min (−30 min), after irradiation for 0, 20, and 40 min under visible light irradiation. (a) S1 and (b) S2.

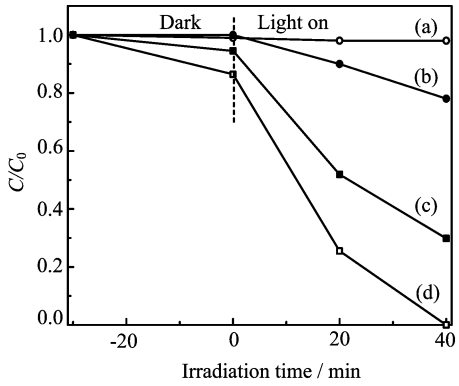

FIG. 6 Photodegradation efficiencies of Rh B as a function of irradiation time for different photocatalysts. (a) Without any catalyst, (b) P25 TiO_2, (c) S2, and (d) S1.

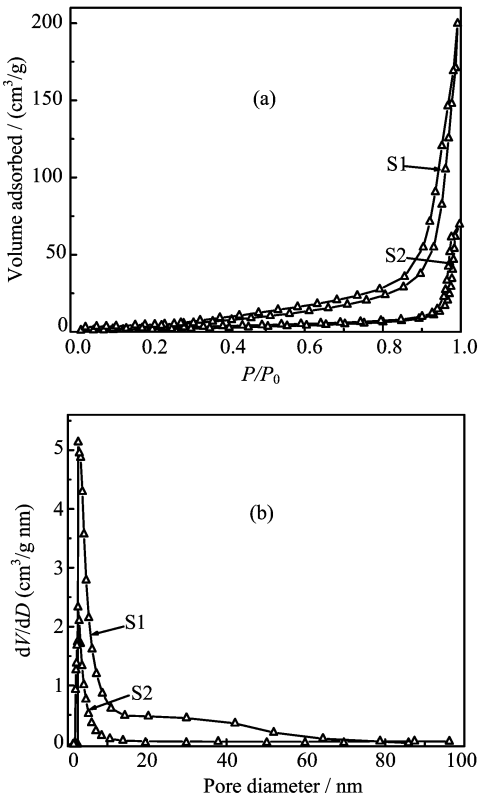

FIG. 7 (a) N_2 adsorption-desorption isotherm curves and (b) pore size distribution of the as-prepared $InVO_4$ samples.

ples is displayed in Fig.6. For comparison, the photodegradation of Rh B by P25 and that without any catalyst were also carried out. The blank test demonstrated that the degradation of Rh B was extremely slow without any photocatalyst under visible-light illumination. From the catalytic studies, $InVO_4$ samples were found to be more photoactive towards Rh B solution than P25 TiO_2. The photolysis test showed that the degradation rate of S1 increased to 100% after 40 min irradiation, much higher than S2. The vastly different photodegradation rates of Rh B by different $InVO_4$ samples indicated that the p-hotocatalytic performances of the as-prepared $InVO_4$ samples were greatly different and strongly dependent on their morphologies. The S1 sample revealed a higher photocatalytic activity which may be associated with the extension to visible light in absorption spectrum (Fig.4), and the smaller grain sizes of the building blocks of the 3D hierarchical structures than that of the 1D nanowires.

According to the above analysis, S1 with higher photocatalytic activity should have a larger surface area than S2. Therefore, the BET surface areas of $InVO_4$ samples were determined to test this hypothesis. N_2 adsorption-desorption isotherms were performed to determine the surface areas of the as-prepared $InVO_4$ samples, as shown in Fig.7(a). The as-fabricated $InVO_4$ samples exhibited a type-IV isotherm, which is a more efficient photocatalyst structure for degradating organic pollutants in water. The BET surface area of S1 (18.11 m^2/g) was about 3 times as large as S2 (6.72 m^2/g). In addition, the corresponding pore size distribution curves for the as-prepared $InVO_4$ samples were obtained by the BJH method, as illustrated in Fig.7(b). The pore size distribution center of S1 is about 3 nm based on BJH desorption pore distribu-

DOI:10.1063/1674-0068/27/04/428-432

tion, which is much higher than S2. The larger BET surface area and porous structure can facilitate more efficient contact of S1 with organic contaminants and thus improve its photocatalytic activity. In addition, several differences in half-widths and intensities of the diffraction peaks were observed in the XRD patterns of $InVO_4$ synthesized at different conditions (Fig.1), indicating that slight changes in the structure, even though all the powders exhibited the orthorhombic structure.

FESEM image of the as-prepared S1 sample after photocatalysis reaction shows that no significant change of the morphology of the S1 sample was detected after catalysis reaction. It demonstrated that the S1 sample had good stability.

IV. CONCLUSION

$InVO_4$ hierarchical microspheres and $InVO_4$ nanowires were successfully synthesized by a facile hydrothermal method. Photocatalytic evaluation revealed that the as-prepared $InVO_4$ photocatalysts exhibited higher photocatalytic activities in the degradation of Rh B under visible-light irradiation (λ>420 nm) compared with commercial P25 TiO_2. Furthermore, the as-synthesized $InVO_4$ hierarchical microspheres showed higher photocatalytic activity than that of $InVO_4$ nanowires. For the degradation of Rh B under visible-light irradiation (λ>420 nm), almost 100% of the Rh B was degraded within 40 min visible-light irradiation. The photocatalytic performance of $InVO_4$ were greatly dependent on the structure and the morphology.

V. ACKNOWLEDGMENTS

This work was supported by the National Natural Science Fundation of China (No.61308095), the China Postdoctoral Science Foundation (No.2013M531286), and the Science Development Project of Jilin Province (No.20130522071JH and No.20130102004JC).

[1] S. Y. Lu, D. Wu, Q. L. Wang, J. H. Yan, A. G. Buekens, and K. F. Cen, Chemosphere **82**, 1215 (2011).
[2] C. X. Huang, K. R. Zhu, M. Y. Qi, Y. L. Zhuang, and C. Cheng, J. Phys. Chem. Solids **73**, 757 (2012).
[3] A. Hasanpour, M. Niyaifar, H. Mohammadpour, and J. Amighian, J. Phys. Chem. Solids **73**, 1066 (2012).
[4] S. H. Shen Chan, T. Y. Wu, J. C. Juan, amd C. Y. Teha, J. Chem. Technol. Biotechnol. **86**, 1130 (2011).
[5] Y. B. Mao and S. S. Wong, J. Am. Chem. Soc **128**, 8217 (2006).
[6] F. Chen, W. W. Zou, W. W. Qu, and J. L. Zhang, Catal. Commun **10**, 1510 (2009).
[7] S. Wang, L. X. Yi, J. E. Halpert, X. Y. Lai, Y. Y. Liu, H. B. Cao, R. B. Yu, D. Wang, and Y. L. Li, Small **8**, 265 (2012).
[8] N. L. Yang, Y. Y. Liu, H. Wen, Z. Y. Tang, H. J. Zhao, Y. L. Li, and D. Wang, ACS Nano **7**, 1504 (2013).
[9] Y. Lin, Z. G. Geng, H. B. Cai, L. Ma, J. Chen, J. Zeng, N. Pan, and X. Q. Wang, Eur. J. Inorg. Chem. **28**, 4439 (2012).
[10] L. B. Wang, Y. C. Wang, R. He, A. W. Zhuang, X. P. Wang, J. Zeng, and J. G. Hou, J. Am. Chem. Soc **135**, 1272 (2013).
[11] J. Zeng and Y. N. Xia, Nature Nanotech **7**, 415 (2012).
[12] Y. Wang, H. X. Dai, J. G. Deng, Y. X. Liu, Z. X. Zhao, X. W. Li, and H. Arandiyan, Chem. Eng. J. **226**, 87 (2013).
[13] T. Yang and D. G. Xia, J. Cryst. Growth **311**, 4505 (2009).
[14] Y. Yan, F. P. Cai, Y. Song, and W. D. Shi, Chem. Eng. J. **233**, 1 (2013).
[15] Z. H. Ai, L. Z. Zhang, and S. C. Lee, J. Phys. Chem. C **114**, 18594 (2010).
[16] C. M. Zhang, Z. Y. Cheng, P. P. Yang, Z. H. Xu, C. Peng, G. G. Li, and J. Lin, Langmuir **25**, 13591 (2009).
[17] J. Ye, Z. Zou, H. Arakawa, M. Oshikiri, M. Shimoda, A. Matsushita, and T. Shishido, J. Photochem. Photobiol. A **148**, 79 (2002).
[18] M. Touboul and P. Toledano, Acta Crystallogr. Sect. B: Struct. Sci **36**, 240 (1980).
[19] H. B. Fang, M. X. Xu, L. Ge, and Z. Y. He, Trans. Nonferrous Met. Soc. China **16**, s373 (2006).
[20] G. Xiao, D. Li, X. Fu, X. Wang, and P. Liu, J. Chin. Inorg. Chem. **20**, 195 (2004).
[21] Y. Li, M. Cao, and L. Feng, Langmuir **25**, 17051712 (2009).
[22] S. C. Yee, R. S. Zhao, Y. T. Yeou, W. Sean, and L. C. Hao, Opt. Mater. **33**, 375380 (2011).
[23] L. X. Xu, L. X. Sang, C. F. Ma, W. Y. Lu, F. Wang, Q. W. Li, H. X. Dai, H. He, and J. H. Sun, Chin. J. Catal. **27**, 100102 (2006).
[24] S. M. Sun, W. Z. Wang, L. Zhou, and H. L. Xu, Ind. Eng. Chem. Res **48**, 1735 (2009).
[25] A. Kudo, I. Tsuji, and H. Kato, Chem. Commun **48**, 1958 (2002).

DOI:10.1063/1674-0068/27/04/428-432